Supplementary Information for

Time-Resolved Atomic Mechanisms of Nickel Oxide Transformations

Emerson C. Kohlrausch,[1] Christopher Leist,[2] Gazi N. Aliev,[3] Zhiqing Ge,[4] Fanyi Zhao,[4] Kecheng Cao,[4] Wolfgang Theis,[3] Ute Kaiser,[2] Jesum Alves Fernandes,[1]* Andrei N. Khlobystov[1]**

[1] School of Chemistry, University of Nottingham, University Park, Nottingham, NG7 2RD, UK
[2] Electron Microscopy Group of Materials Science, Ulm University, Ulm, 89081, Germany
[3] School of Physics & Astronomy, University of Birmingham, Birmingham, UK, B15 2TT
[4] School of Physical Science and Technology and Shanghai Key Laboratory of High-Resolution Electron Microscopy, Shanghai Tech University, Shanghai, People's Republic of China

*Corresponding authors: andrei.khlobystov@nottingham.ac.uk
jesum.alvesfernandes@nottingham.ac.uk
ute.kaiser@uni-ulm.de

This file includes:

Supplementary Fig. 1 to 8

Other Supplementary Information for this manuscript includes the following:

Supplementary Movies 1 to 6

Supplementary Movies Captions

Supplementary Movie 1 | Electron-beam-induced reduction of NiO over a large irradiated area. Cc/Cs-corrected HRTEM multiframe movie showing the progressive transformation of crystalline NiO particles into disordered metallic Ni under high electron-beam flux. The movie illustrates the large-area response of NiO particles to electron irradiation, with progressive loss of the crystalline NiO lattice as reduction proceeds.

Supplementary Movie 2 | Atomic-scale reduction of a selected NiO nanocrystal. Cc/Cs-corrected HRTEM multiframe movie showing the progressive reduction of the NiO nanocrystal analysed in Fig. 2, together with the corresponding fast Fourier transforms (FFTs). Oxygen removal initiates preferentially at the particle edges and progresses inwards, accompanied by lattice rearrangement and loss of crystallinity. The corresponding FFTs show the progressive disappearance of the NiO crystallographic reflections, revealing the transition from crystalline NiO to a disordered, amorphous Ni-rich cluster.

Supplementary Movie 3 | NiO nucleation at a graphene step edge (region 1). Cc/Cs-corrected HRTEM multiframe movie showing the nucleation of NiO at a graphene step edge, corresponding to the region analysed in Fig. 3c. Subcritical crystalline NiO nuclei repeatedly form and disassemble until a nucleus containing approximately 4–5 projected NiO lattice units is established, after which sustained crystal growth occurs.

Supplementary Movie 4 | NiO nucleation (region 2). Cc/Cs-corrected HRTEM multiframe movie showing NiO nucleation within an amorphous cluster supported on graphene, corresponding to the region analysed in Fig. 3d. The sequence reveals repeated formation and dissolution of subcritical NiO domains, followed by sustained growth once the crystalline nucleus reaches approximately 4–5 projected NiO lattice units.

Supplementary Movie 5 | Step-edge-mediated growth and edge dynamics of NiO. Cc/Cs-corrected HRTEM multiframe movie corresponding to Fig. 4, showing sustained growth of a NiO crystal from an adjacent amorphous Ni-rich region. Growth proceeds preferentially at atomic steps along {100}-type NiO edges and is accompanied by dynamic atomic attachment, detachment, migration, and rearrangement at the crystal boundary. These processes progressively reconstruct and smooth the NiO edge towards a lower-energy configuration.

Supplementary Movie 6 | Rotation-mediated sintering of NiO particles. Cc/Cs-corrected HRTEM multiframe movie showing the sintering of neighbouring NiO particles through in-plane rotation, interfacial reconstruction, and lattice merging, corresponding to the process analysed in Fig. 5. The relative crystallographic misorientation decreases as the particles rotate, enabling the formation of a stable crystalline junction and subsequent sintering of the NiO domains.

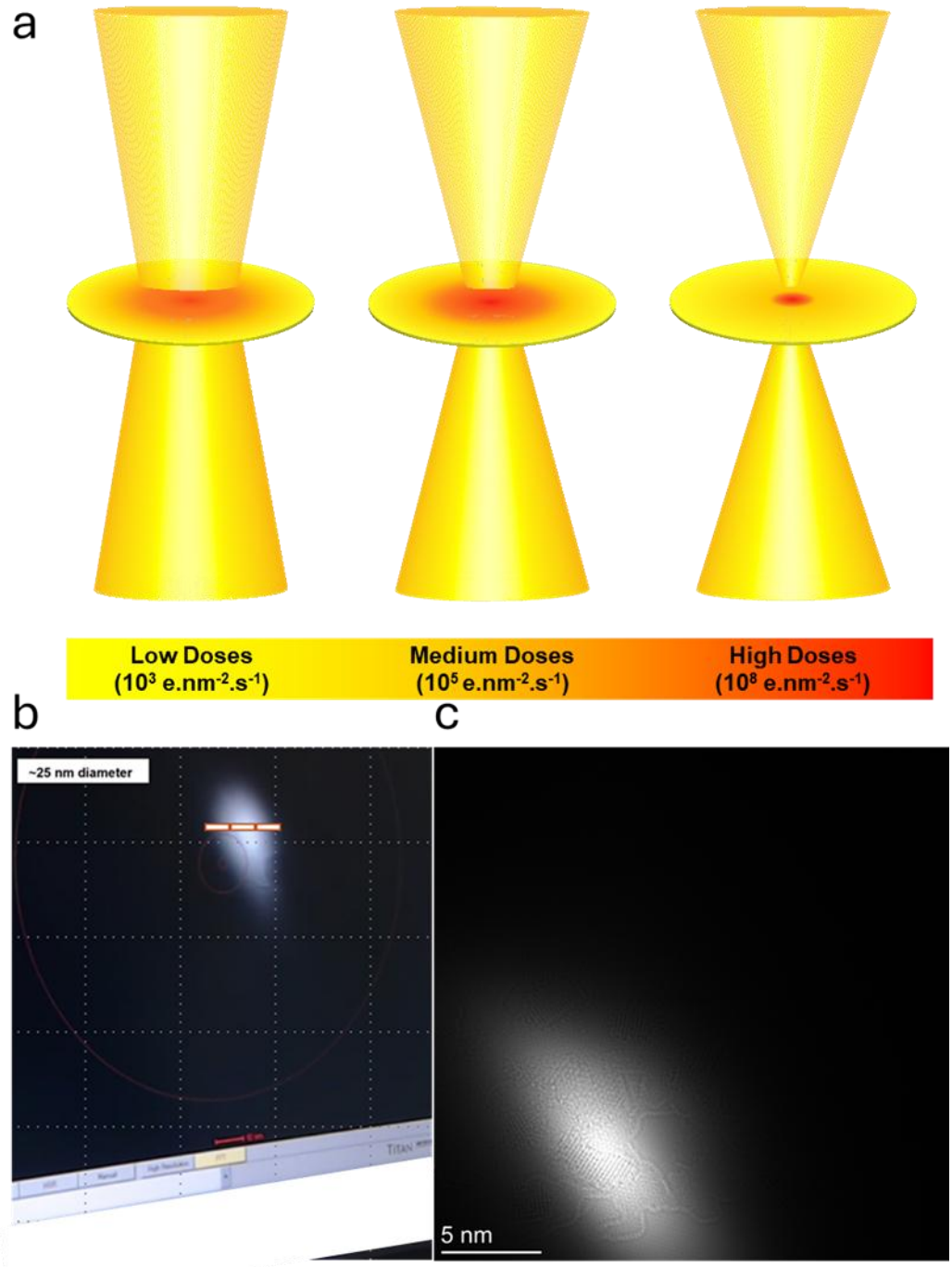

Supplementary Fig. 1 | Beam-size–controlled electron flux for in situ imaging (a) Illustration of the approach used to tune the electron flux by changing the size of the illuminated area. **(b)** Image of the microscope view screen on the control monitor during high-flux irradiation, showing the electron beam confined to a small region of the sample. **(c)** 60 keV Cc/Cs-corrected HRTEM image acquired under high-flux conditions. The electron beam was focused onto the nanocluster region to increase the local electron flux, while short exposure times were used for image acquisition.

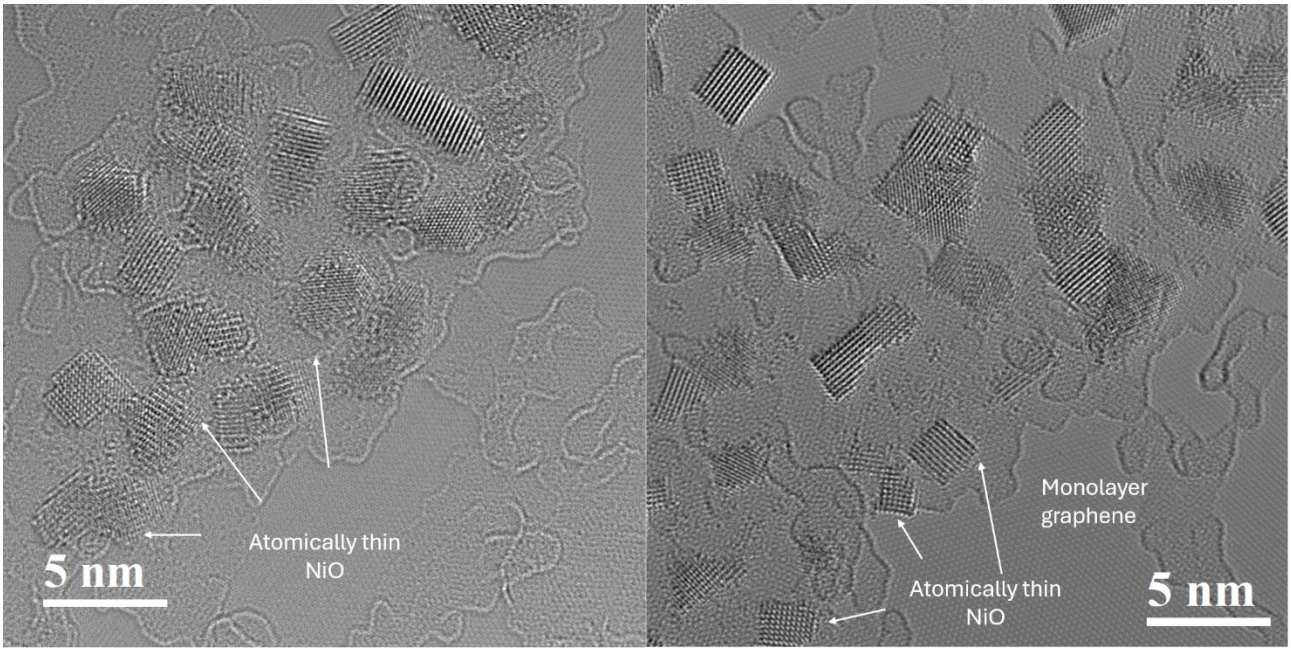

Supplementary Fig. 2 | Atomically thin NiO nanocrystals supported on monolayer graphene. Cc/Cs-corrected HRTEM images showing atomically thin NiO nanocrystals dispersed on monolayer graphene. The NiO domains display clear lattice fringes and predominantly rectangular morphologies, consistent with crystalline NiO confined to few-layer thickness. Arrows highlight representative atomically thin NiO particles, while the low-contrast background corresponds to the graphene support.

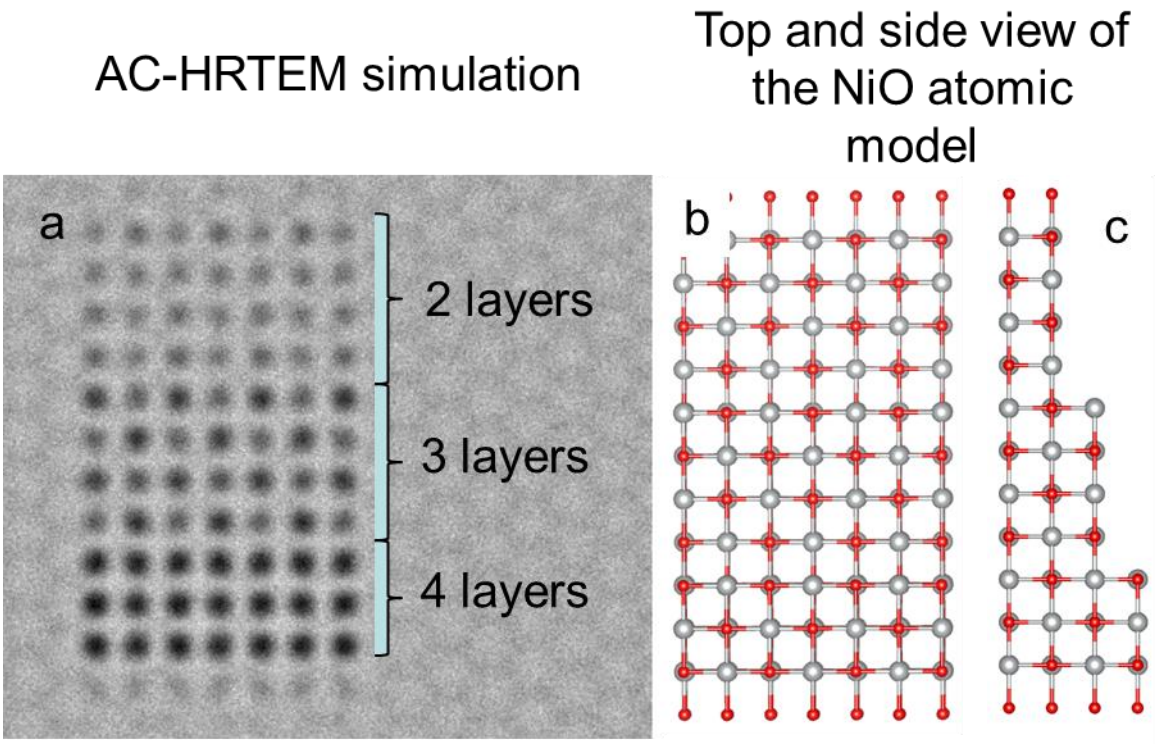

Supplementary Fig. 3 | Simulated Cc/Cs-corrected HRTEM contrast for NiO with varying atomic thickness (a) Simulated Cc/Cs-corrected HRTEM image of a NiO projection with varying thicknesses, showing regions corresponding to 2, 3, and 4 atomic layers. (b) Top view and (c) side view of the NiO atomic model used in the simulation. The comparison suggests that the observed NiO structure is consistent with the experimentally observed atomically thin configuration.

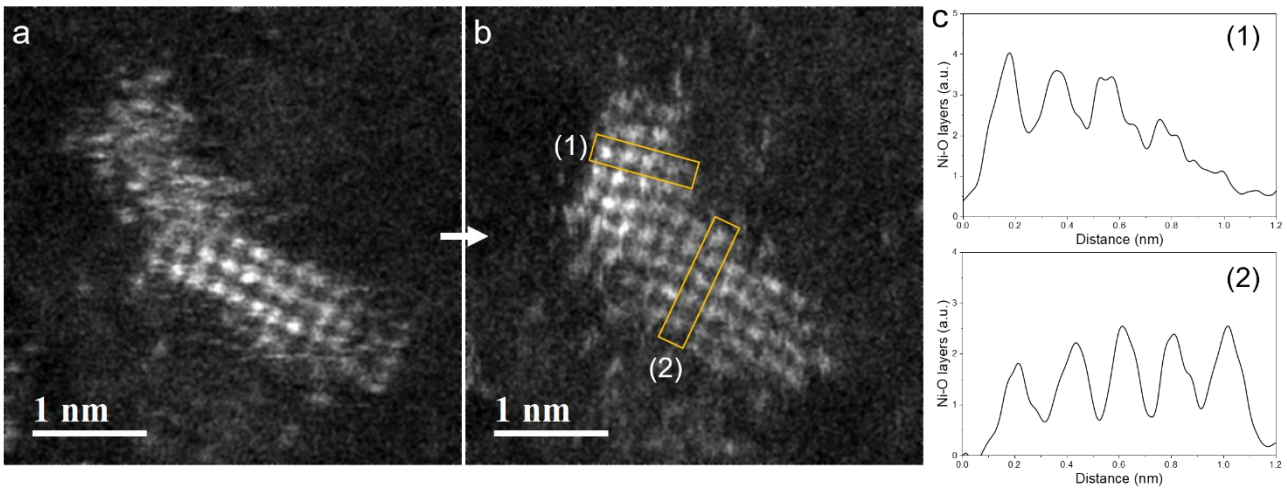

Supplementary Fig. 4 | Electron-beam-induced crystallisation and thickness analysis of atomically thin NiO. a,b, Sequential AC-STEM images of the same NiO/Ni region. The first scan shows a crystalline rock-salt NiO domain attached to an amorphous Ni-rich region. After a second scan, the amorphous region becomes partially ordered, indicating beam-promoted crystallisation/oxidation into NiO. Yellow boxes highlight newly formed lattice fringes with different local orientations. **c,** Column-intensity analysis of the NiO lattice, showing distinct intensity levels corresponding to regions with approximately one and two projected Ni–O units (two and four atomic planes, respectively).

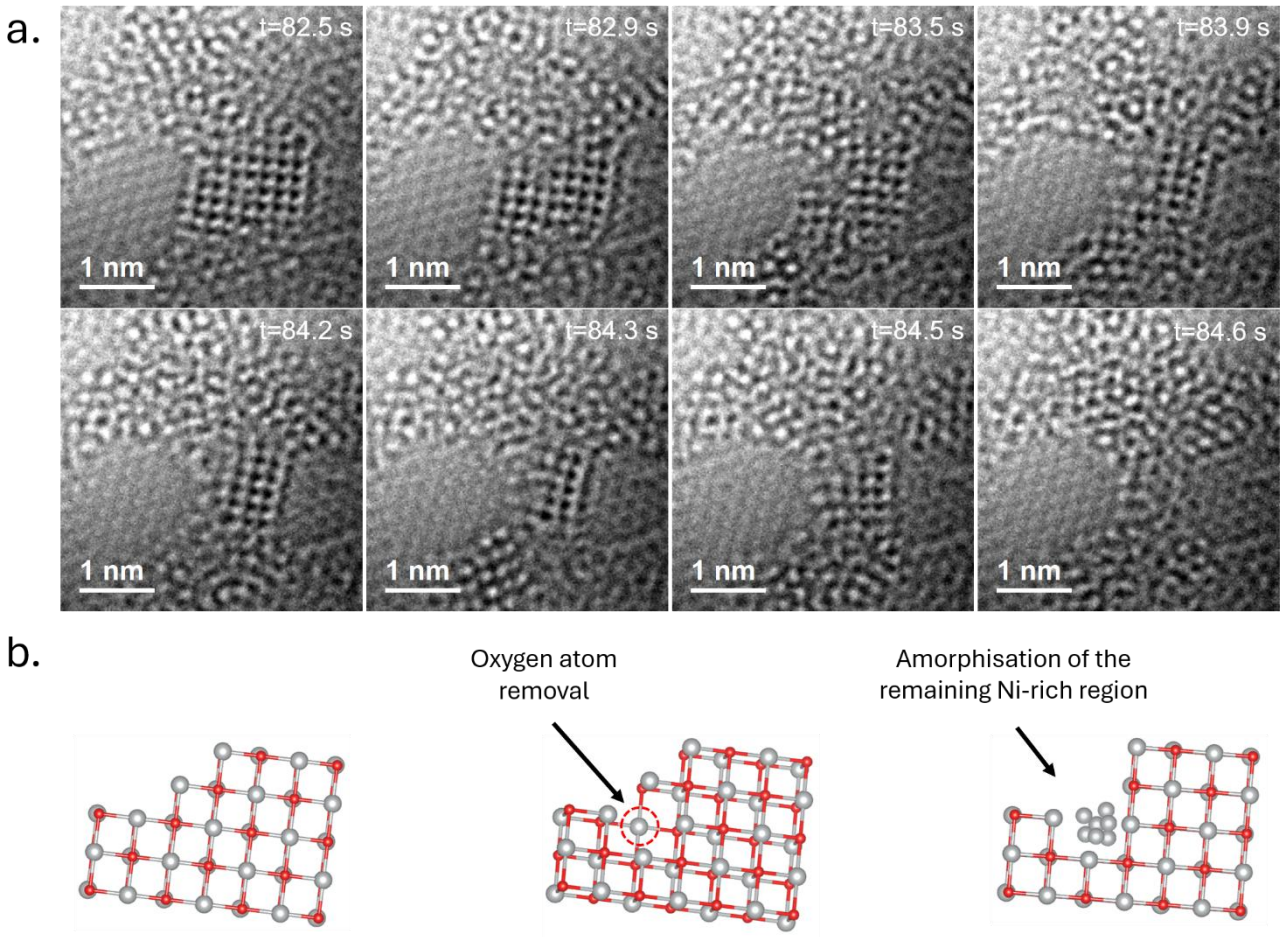

Supplementary Fig. 5 | Edge-initiated oxygen removal during NiO reduction. a, Time-resolved Cc/Cs-corrected HRTEM images showing the progressive reduction of a NiO nanocrystal, initiated at an under-coordinated edge site and followed by lattice distortion and loss of crystallinity. **b,** Corresponding structural models illustrating oxygen removal from the edge, subsequent local lattice rearrangement, and amorphisation of the remaining Ni-rich region

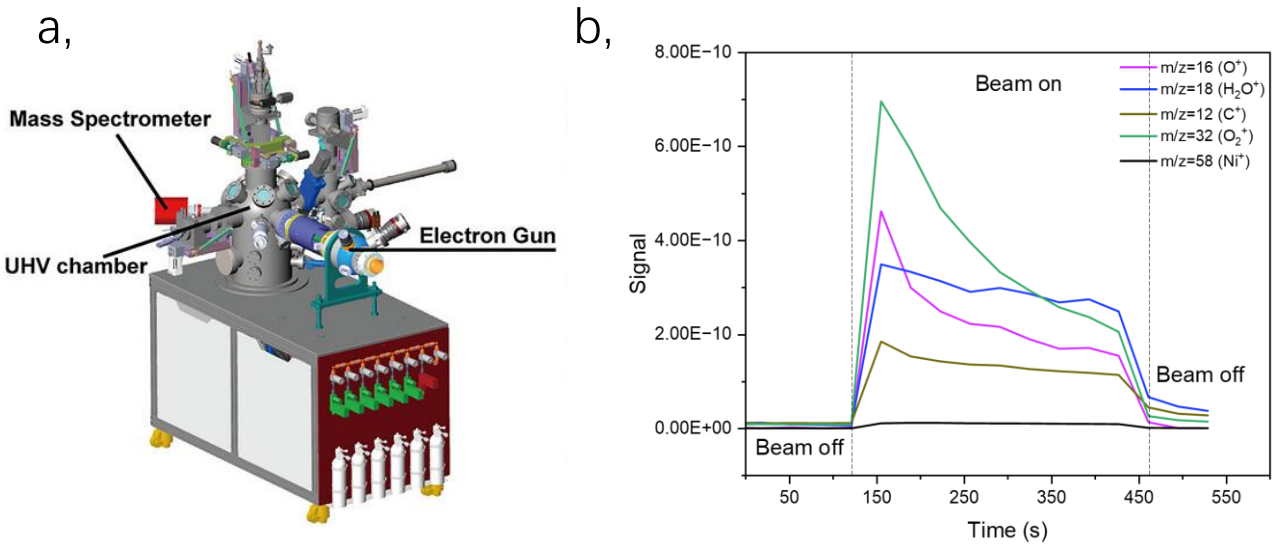

Supplementary Fig. 6 | Electron-beam mass-spectrometry analysis of NiO. a, Schematic of the EB–MS apparatus, comprising an electron gun and mass spectrometer integrated into an ultra-high-vacuum chamber. **b,** Time-dependent mass-spectrometric signals recorded before, during and after electron-beam irradiation of NiO deposited on graphite-supported holey-carbon Cu TEM grids. The detected signals correspond to *m/z* = 16 (O^+), 18 (H_2O^+), 12 (C^+), 32 (O_2^+), 44 (CO_2^+) and 58 (Ni^+).

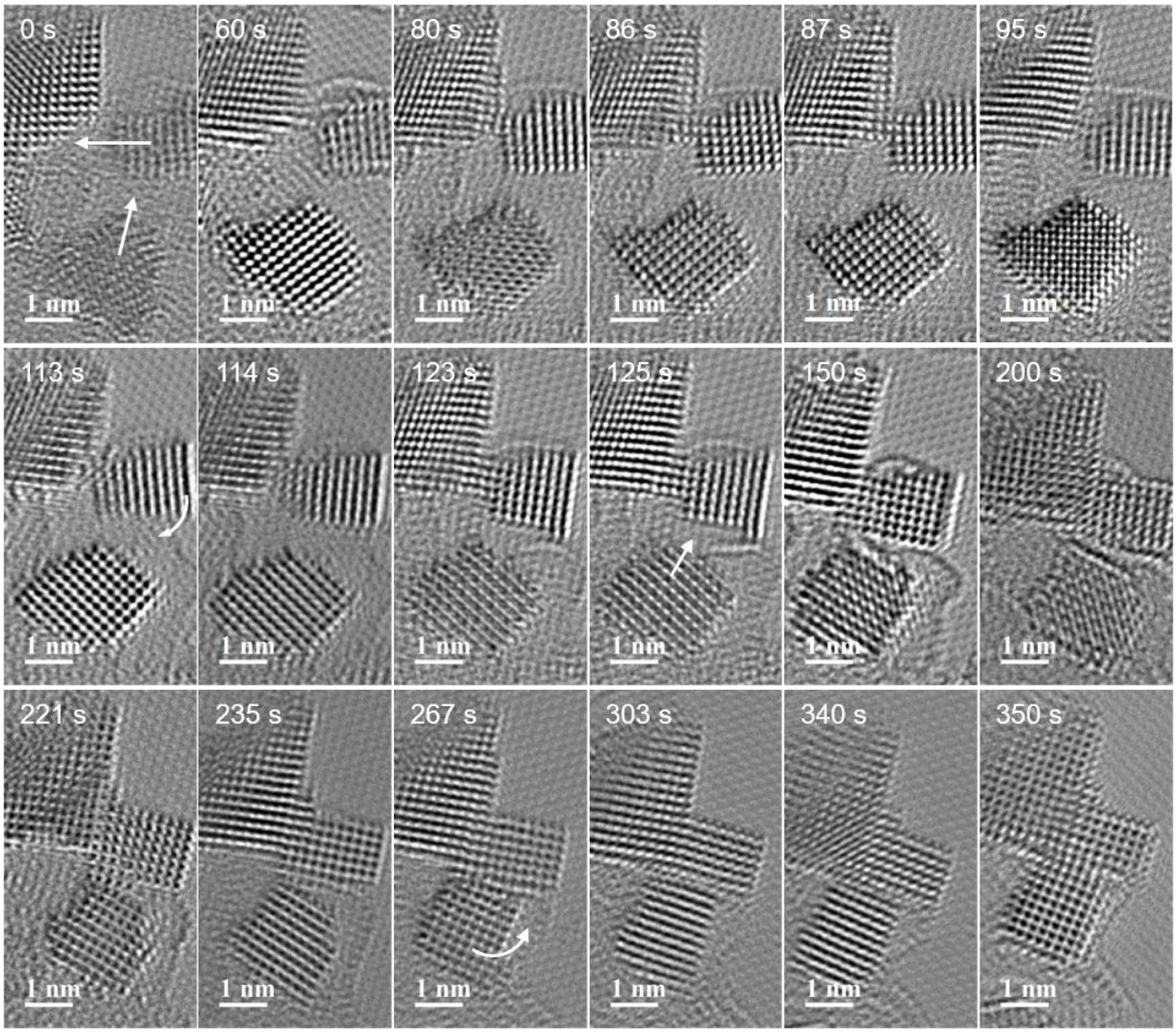

Supplementary Fig. 7 | In-plane rotation-mediated merging of NiO particles. Time-resolved Cc/Cs-corrected HRTEM image sequence showing the coalescence of neighbouring NiO particles through in-plane rotation and lattice alignment. Initially, the particles are separated and display different crystallographic orientations. During imaging, the mobile particle rotates progressively, as indicated by the arrows, reducing the angular mismatch with the adjacent NiO domain. Once the lattice orientations become compatible, an interparticle neck forms, followed by further structural rearrangement and consolidation into a larger crystalline NiO domain. This sequence demonstrates that particle merging proceeds through rotation-assisted oriented attachment followed by interface reconstruction.

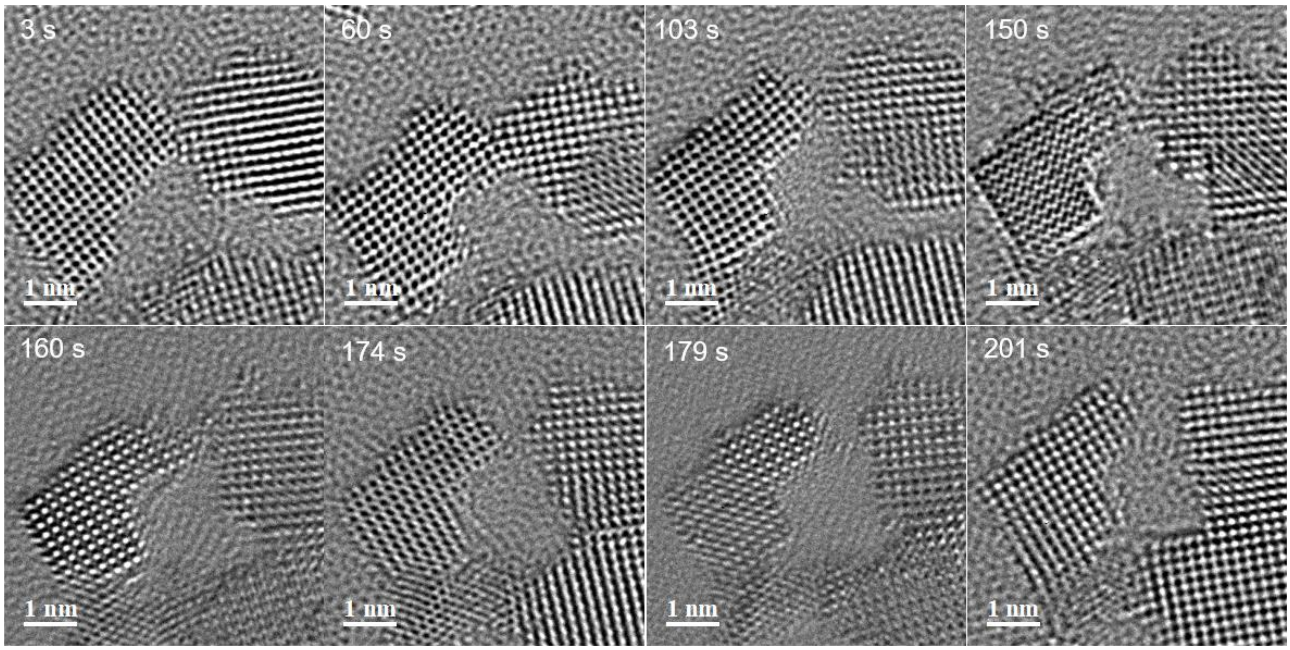

Supplementary Fig. 8 | Failed oriented attachment between misaligned NiO particles. Time-resolved Cc/Cs-corrected HRTEM images show two neighbouring NiO domains forming a transient interparticle contact. Because the lattices do not reach a common crystallographic orientation, the contact is unstable and subsequently ruptures, leaving the particles separated.